eLIFE elifesciences.org

RESEARCH ARTICLE

Figures and figure supplements

Retinal stem cells modulate proliferative parameters to coordinate post-embryonic morphogenesis in the eye of fish

Erika Tsingos *et al*

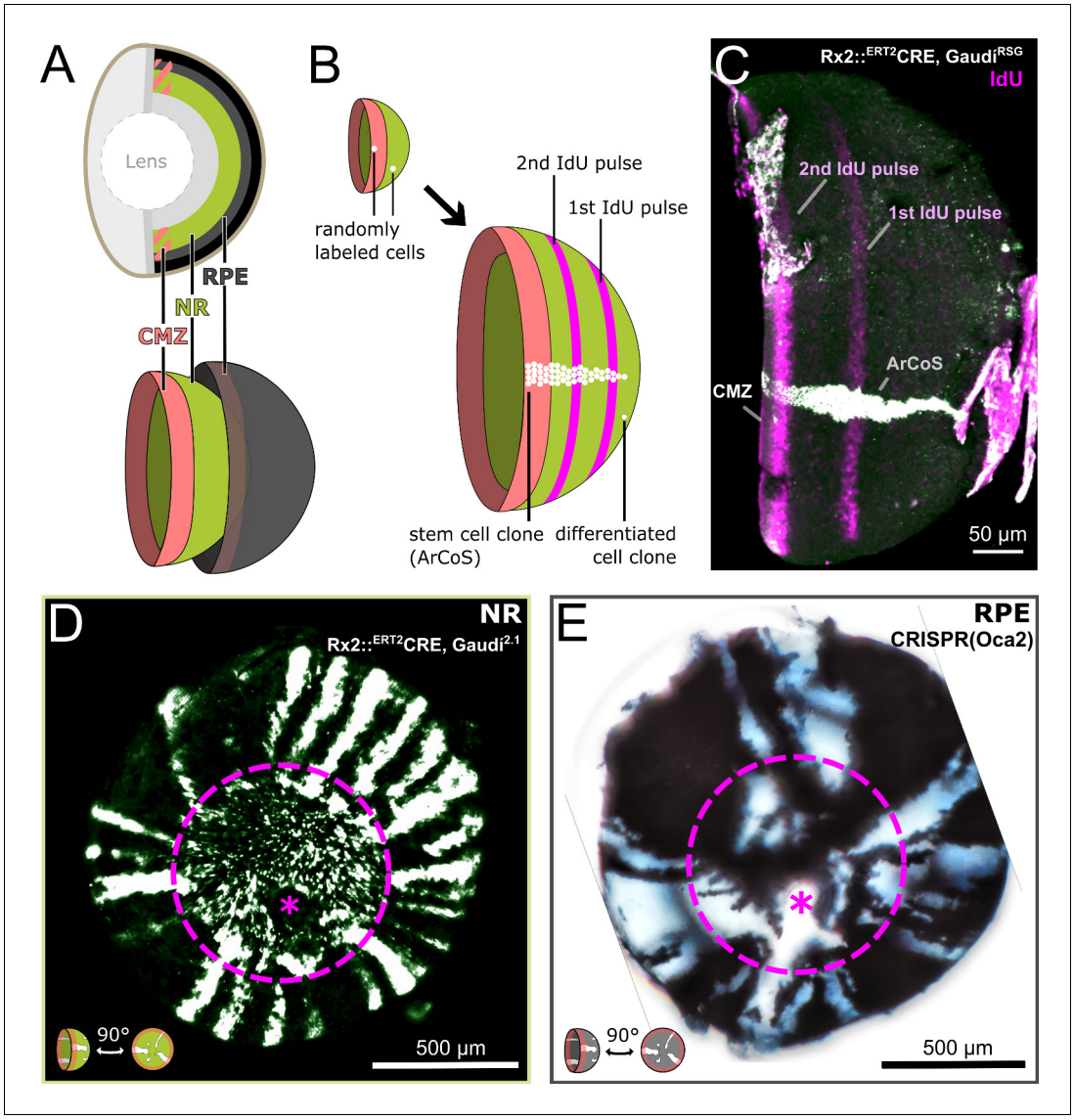

Figure 1. Clonal labelling enables analysis of growth patterns in NR and RPE. (**A**) Schematic anatomy of the fish eye. (**B**) Growth patterns of retinal cell population (concentric rings) and individual clones. (**C**) False color immunostained NR of 3 week old Rx2::^{ERT2}Cre, Gaudí^{RSG} fish with ArCoS and concentric rings of IdU-labelled cells. Overnight IdU pulses were at 1 and 2.5 weeks of age. Leftover undissected autofluorescent tissue fragments cover the far right of the cup-shaped retina. (**D**) Proximal view of clones induced in the NR of Rx2::^{ERT2}Cre, Gaudí$^{2.1}$ fish. Maximum projection of confocal stack of GFP immunostaining in false colors. (**E**) Proximal view of unpigmented lineages induced in the RPE by mosaic bi-allelic knockout of Oca2 using CRISPR/Cas9. Focused projection of brightfield focal stack. Images in (**D**) and (**E**) have been rotated to place the optic nerve exit (pink asterisk) ventrally; the embryonic retina is circled with a pink dashed line.

DOI: https://doi.org/10.7554/eLife.42646.004

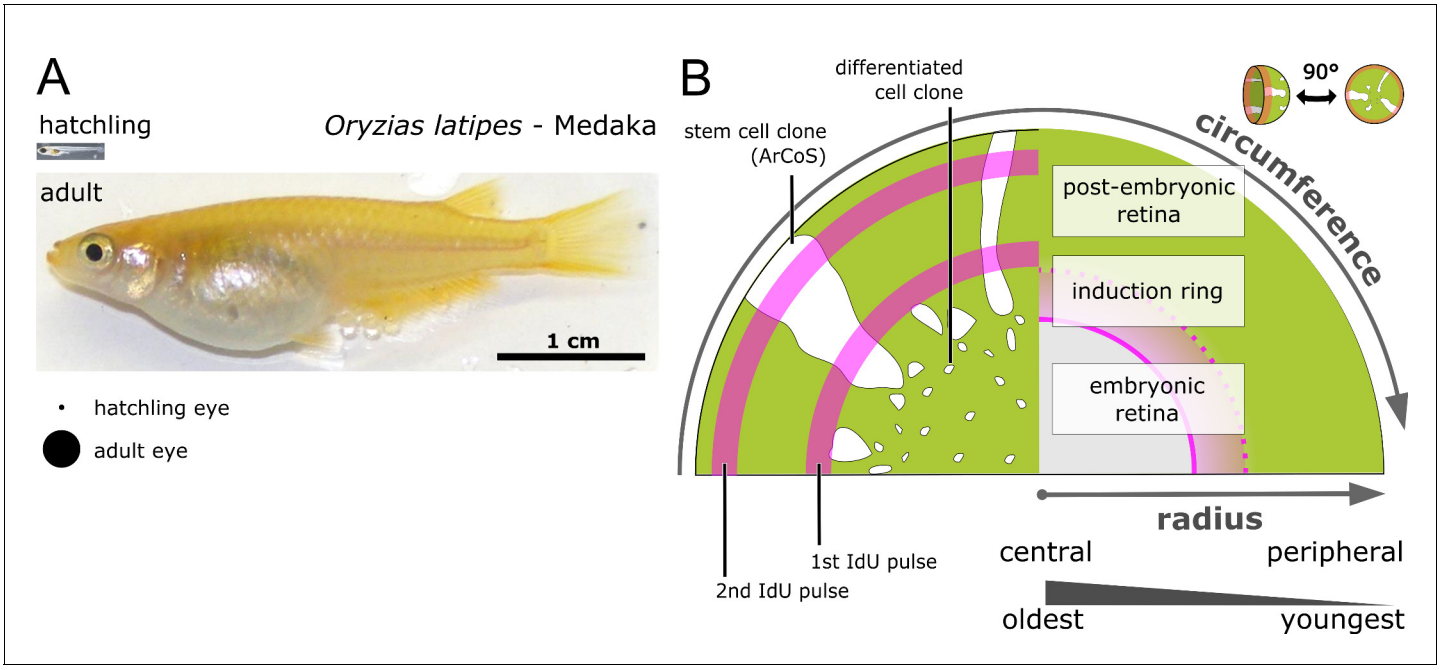

Figure 1—figure supplement 1. The retinal radius represents a temporal axis. (**A**) Photos of newly hatched and young sexually mature adult medaka. The projected area of hatchling and adult eyes is highlighted underneath. (**B**) Schematic drawing of proximal view on clones and IdU 'growth rings' of the NR. The central part of the eye is formed embryonically and contains the oldest cells, while the post-embryonic retina is younger and derives from stem cells in the CMZ, which is located at the extreme periphery. The embryonic retina corresponds to the area of the entire differentiated retina in the hatchling; the induction ring corresponds to the position of the CMZ at the timepoint of Cre recombination.

DOI: https://doi.org/10.7554/eLife.42646.005

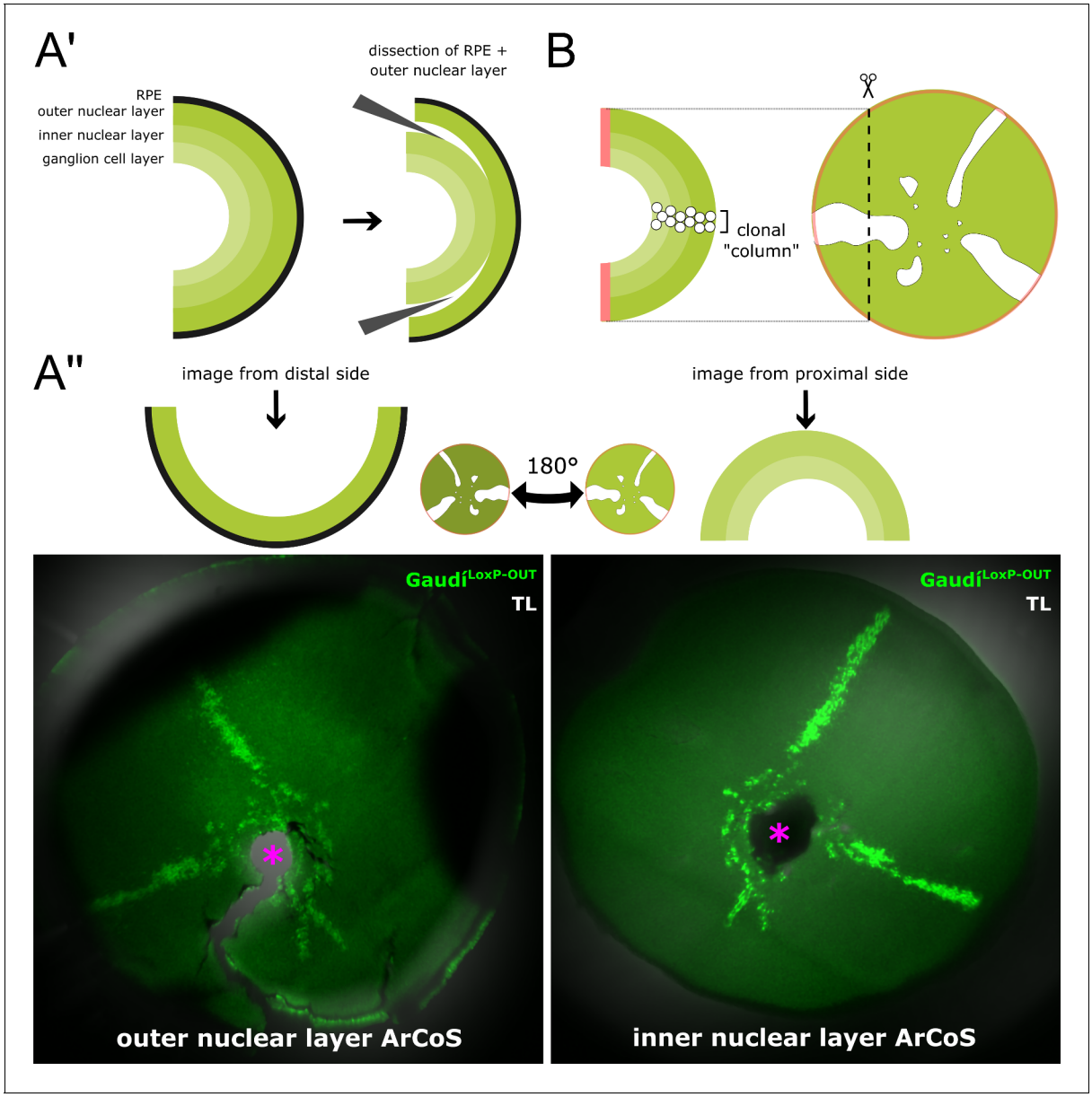

Figure 1—figure supplement 2. NR ArCoS form narrow columns spanning all NR layers. (**A'**) Schematic cross-section of a dissected retina illustrating the various neuronal layers of the NR. The RPE is single-layered. With short fixation times and careful dissection, the RPE and outer nuclear layer can be peeled off from the inner nuclear and ganglion cell layers. (**A''**) Retina dissected from an adult fish that received a transplant of cells from ubiquitously GFP-expressing donors (Gaudí$^{LoxP\text{-}OUT}$) at embryonic blastula stage. NR clones always span all neuronal layers throughout the retinal radius. Maximum projection of confocal stacks of different preparations of the same retina showing endogenous GFP signal and transmitted light (TL). Pink asterisk marks optic nerve exit. (**B**) Schematic cross-section through an NR ArCoS highlighting clonal columns among differentiated retinal progeny.
DOI: https://doi.org/10.7554/eLife.42646.006

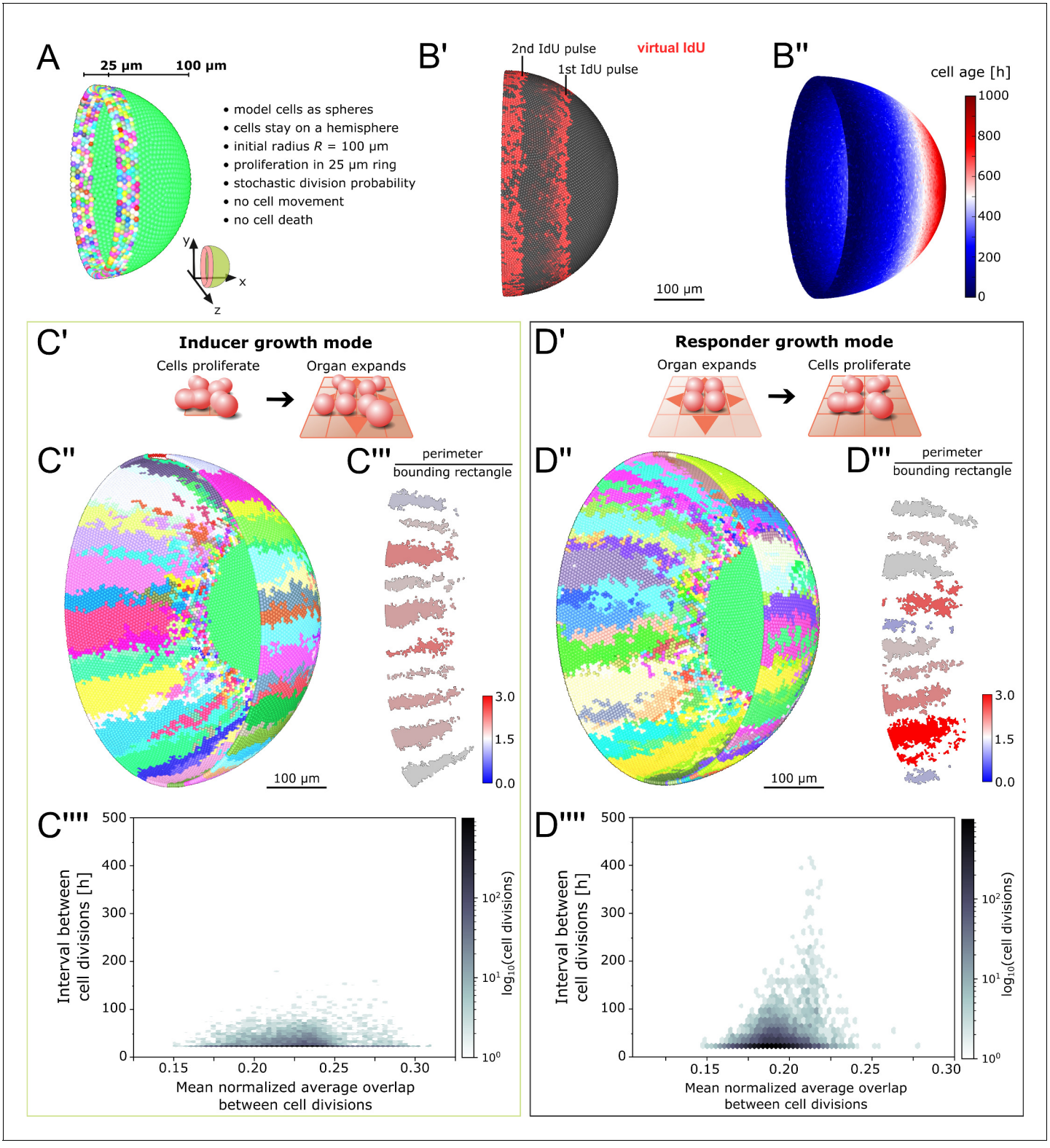

Figure 2. Feedback between proliferation and organ growth affects the simulated clonal pattern. (**A**) Initial condition and properties of the agent based model of the growing fish retina. Virtual embryonic retina in light green. CMZ cells are assigned unique colors for virtual clonal analysis. (**B'**) Simulated IdU pulse-chase experiment. First pulse: 200–220 hr, second pulse: 400–420 hr. Screenshot from 435 hr. Virtual cells incorporate IdU when they divide and half of the signal is passed on to each daughter cell. (**B''**) Cell age (hours elapsed since last cell division) forms a gradient with the oldest cells in the virtual embryonic retina. (**C'**) In the inducer growth mode, the modelled tissue signals upstream to drive growth of other tissues in the organ. (**C''**)

Figure 2 continued on next page

Figure 2 continued

Representative screenshot of inducer growth mode. (**C‴**) Sample of 10 clones from (**C″**). Colors: ratio of full perimeter by bounding rectangle perimeter, a metric for shape complexity. (**C⁗**) Cell division intervals plotted against the mean average overlap. (**D′**) In the responder growth mode, control of the growth of the modelled tissue is downstream of an external signal. (**D″**) Representative screenshot of the responder growth mode. (**D‴**) Sample of 10 clones from (**D″**) evaluated by the same shape metric as in (**C‴**). (**D⁗**) Cell division intervals plotted against the mean average overlap. Note the higher range of values for cells over the threshold overlap of 0.2.

DOI: https://doi.org/10.7554/eLife.42646.007

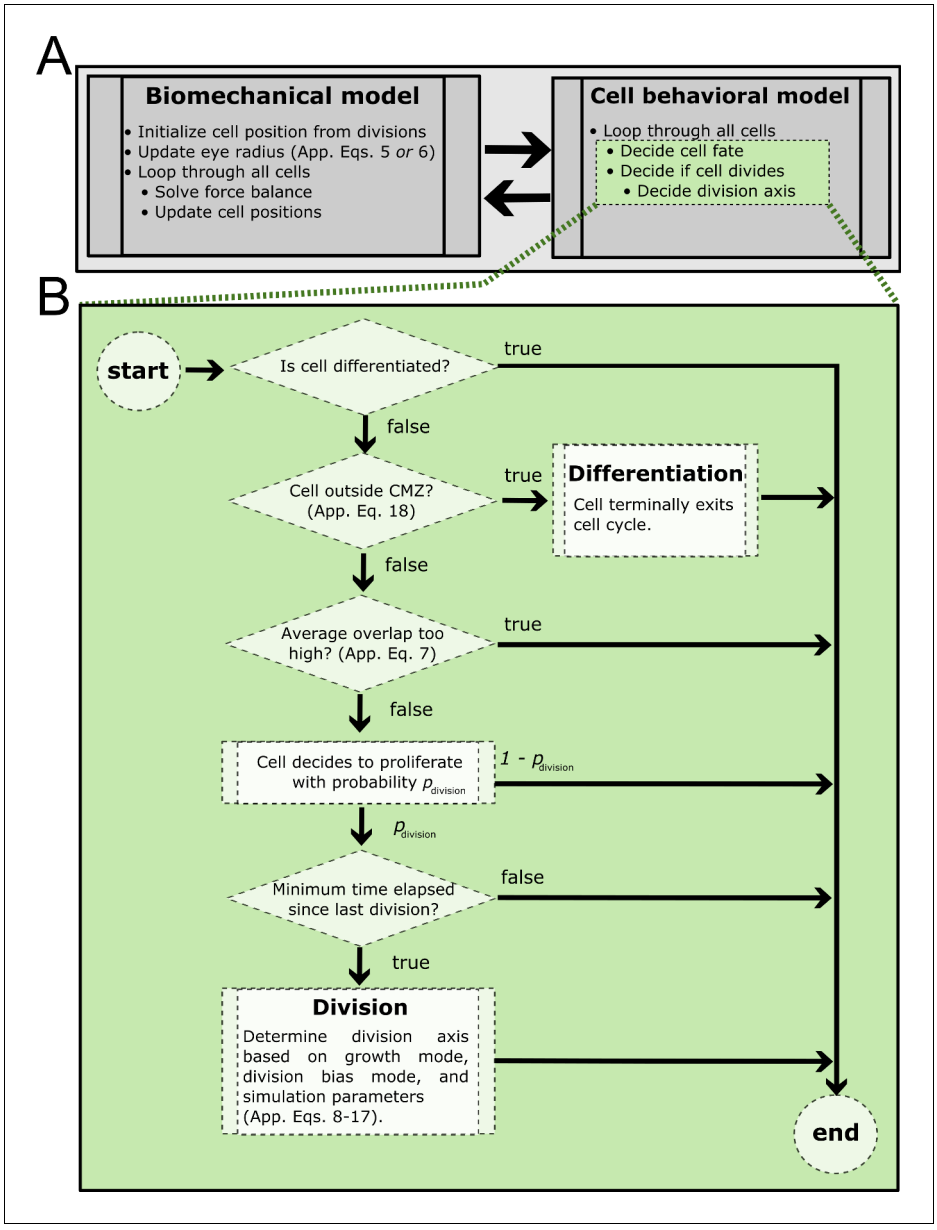

Figure 2—figure supplement 1. Process diagram summarizing model decision tree. (**A**) At every simulation step, the biomechanical model is solved followed by simulation of the cell behavioral model. Green shaded steps expanded in (**B**). (**B**) Summary of cell behavioral decision tree. If a cell decides to divide but the minimum cell cycle time has not elapsed, it will suppress division and check only the other conditions (proliferative cell type, permissive overlap, minimum time elapsed).

DOI: https://doi.org/10.7554/eLife.42646.008

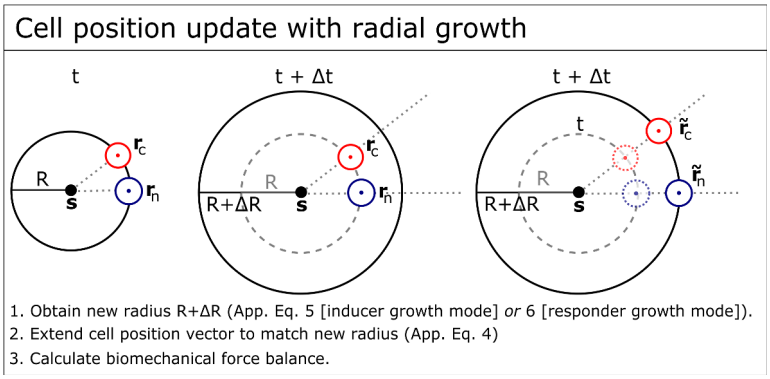

Figure 2—figure supplement 2. Cell position update with radial growth of the simulated retina. To simulate radial growth, the vectors extending from the eye globe's center to the cells' center are extended to match the radius of the growing hemispherical organ. This leads to a decrease in cell density over time as described for growing fish eyes (***Lyall, 1957***; ***Johns, 1977***; ***Ohki and Aoki, 1985***). Additionally, every numerical step of the solver for the biomechanical force-balance includes similar repositioning of all cells, to ensure they stay on the hemispherical surface. Each simulation step includes 100 such iterations.

DOI: https://doi.org/10.7554/eLife.42646.009

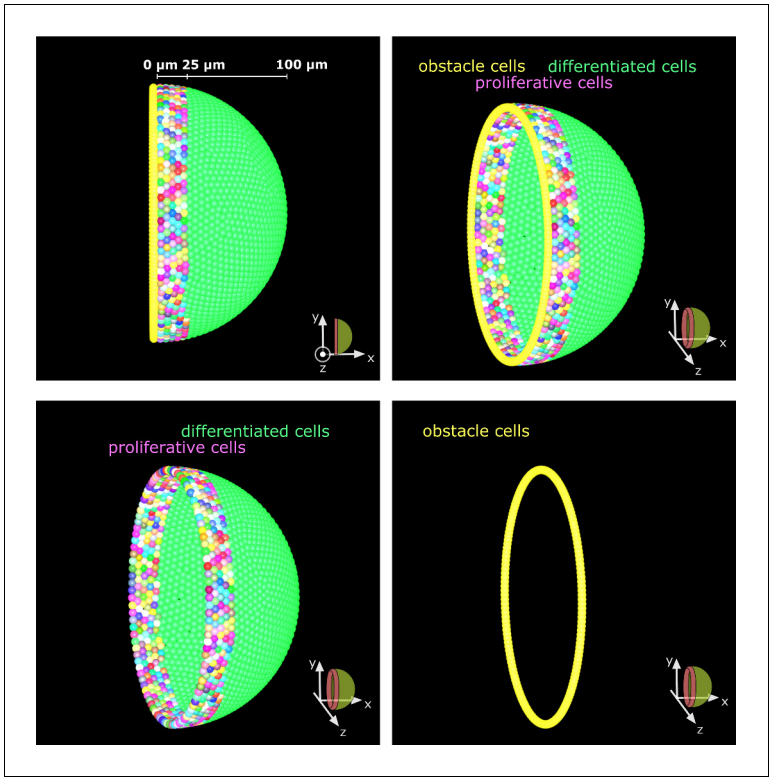

Figure 2—figure supplement 3. Obstacle cells create an impassable boundary at the hemisphere's edge. A single layer of tightly packed cells prevents cell movement beyond the hemispherical edge. These obstacle cells represent the edge of the tissue and have no other influence on the simulation.
DOI: https://doi.org/10.7554/eLife.42646.010

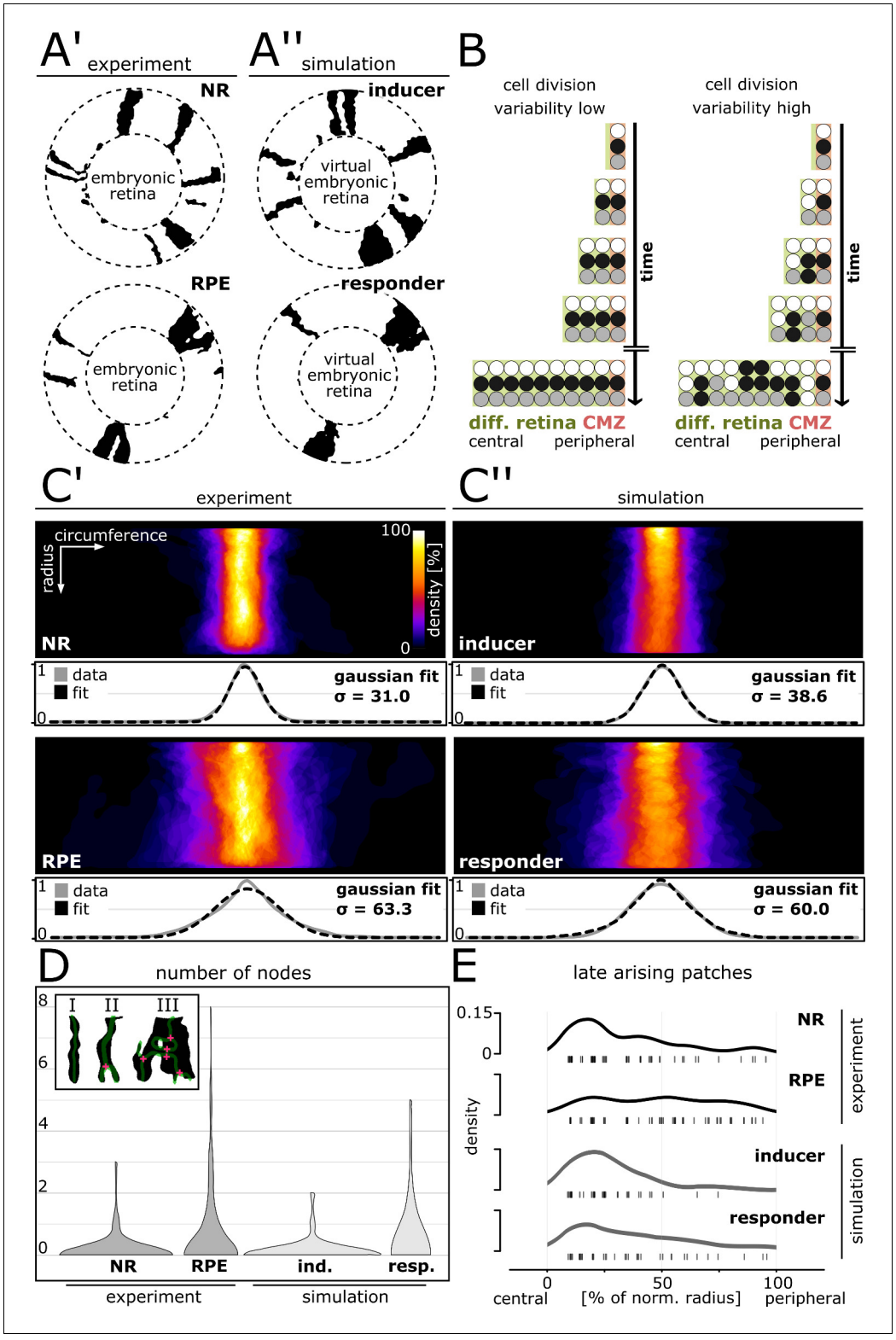

Figure 3. Cell division variability is lower in NR and inducer growth mode, higher in RPE and responder growth mode. (**A'–A''**) Proximal view of segmented patches in adult NR and RPE and simulated patches in inducer and responder growth mode. The central (virtual) embryonic retina was excluded from analysis. (**B**) Different degrees of variability in cell division timing affect the clone pattern. (**C'–C''**) Upper panels: Superposition of labelled patches in the NR (n = 156 patches from seven retinae), RPE (n = 142 patches from 10 retinae), inducer growth mode

Figure 3 continued on next page

Figure 3 continued

(n = 145 patches from five simulations), and responder growth mode (n = 107 patches from five simulations). The radius was normalized to the same length in all samples. Lower panels: Gaussian fits of normalized pixel intensity profiles projected along the vertical axis. σ - Standard deviation of fit. (**D**) Distribution of number of nodes of skeletonized patches. Inset: Examples of patches without nodes (I), with only one node (II), or with multiple nodes (III). (**E**) Rug plot showing number of patches that are not connected to the embryonic retina ('late arising patches') at the respective positions along the normalized radius. NR (n = 54 late patches) and inducer growth mode (n = 35 late patches) display a marked peak in the central portion, while RPE (n = 56 late patches) and responder growth mode (n = 37 late patches) have a more uniform distribution.

DOI: https://doi.org/10.7554/eLife.42646.013

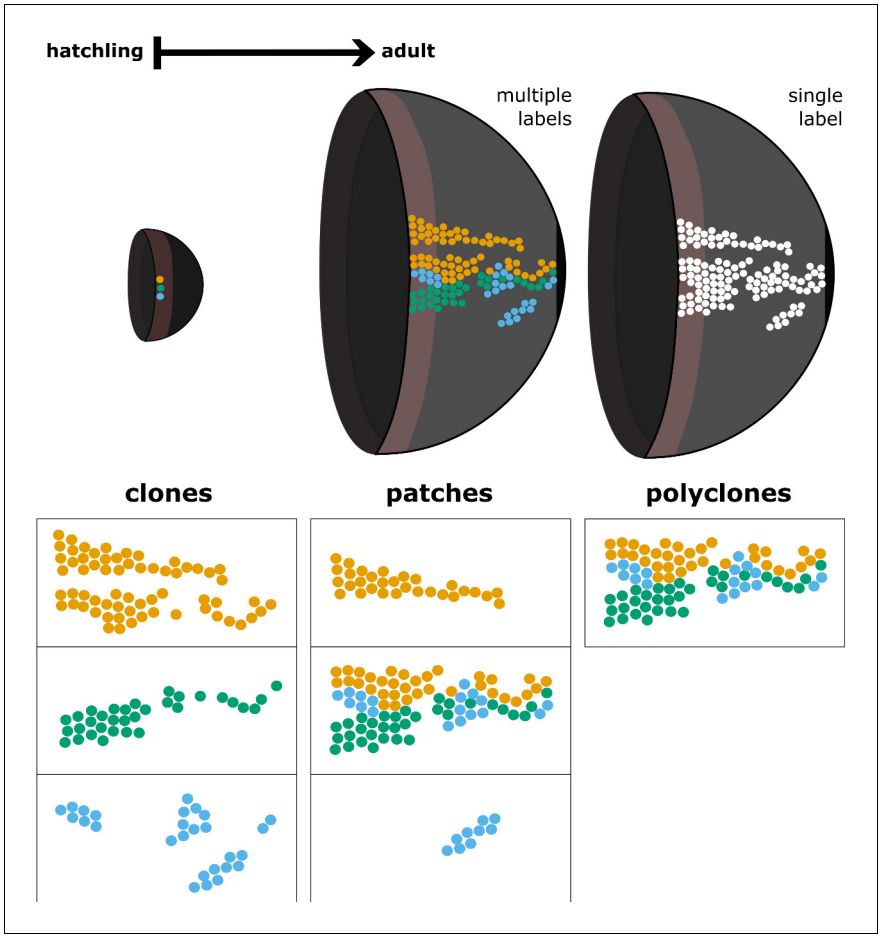

Figure 3—figure supplement 1. Relationship between clones, patches, and polyclones. The term clone denotes lineages derived from a single founder cell, while polyclones are conglomerates of clones that are spatially clustered. We define patches as contiguous domains of labelled cells regardless of their clonal relationship. A patch may represent a clone, a fragment of a clone, or a polyclone.

DOI: https://doi.org/10.7554/eLife.42646.014

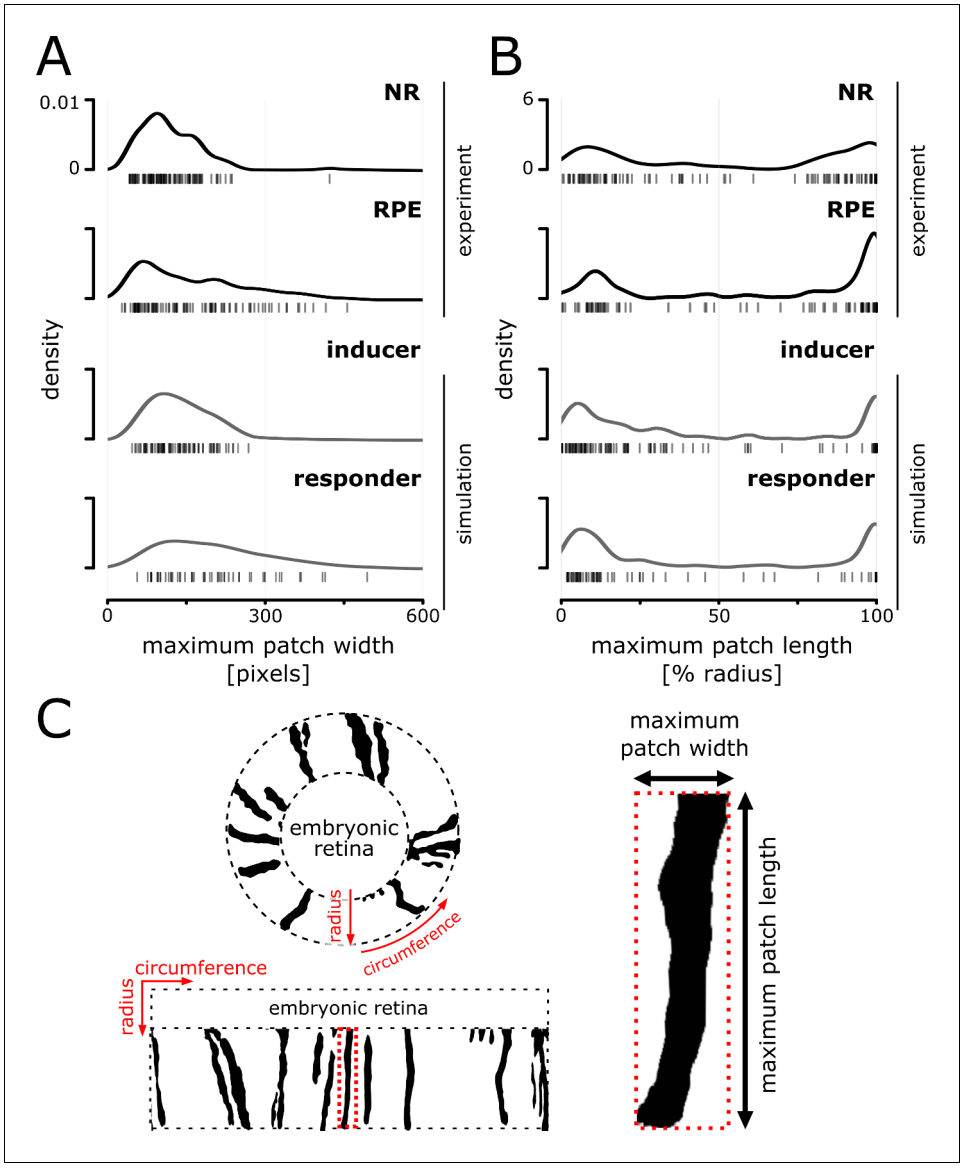

Figure 3—figure supplement 2. Distributions of patch width and length in experiment and simulation. (**A**) Distribution of maximum width of patches that span at least 20% of the radial coordinate. (**B**) Distribution of maximum patch length normalized against the postembryonic retinal radius; late arising patches (central-most pixel after 20% of the radius) were excluded from the analysis. Note the bimodal distribution that results from the abundance of very short and very long patches. (**C**) Illustration of a retina before and after transforming from polar coordinates centered on the embryonic retina to a cartesian representation. Patch bordered in dotted red line is magnified on the right to illustrate the metrics used for plotting distributions in (**A**) and (**B**) of this figure.

DOI: https://doi.org/10.7554/eLife.42646.015

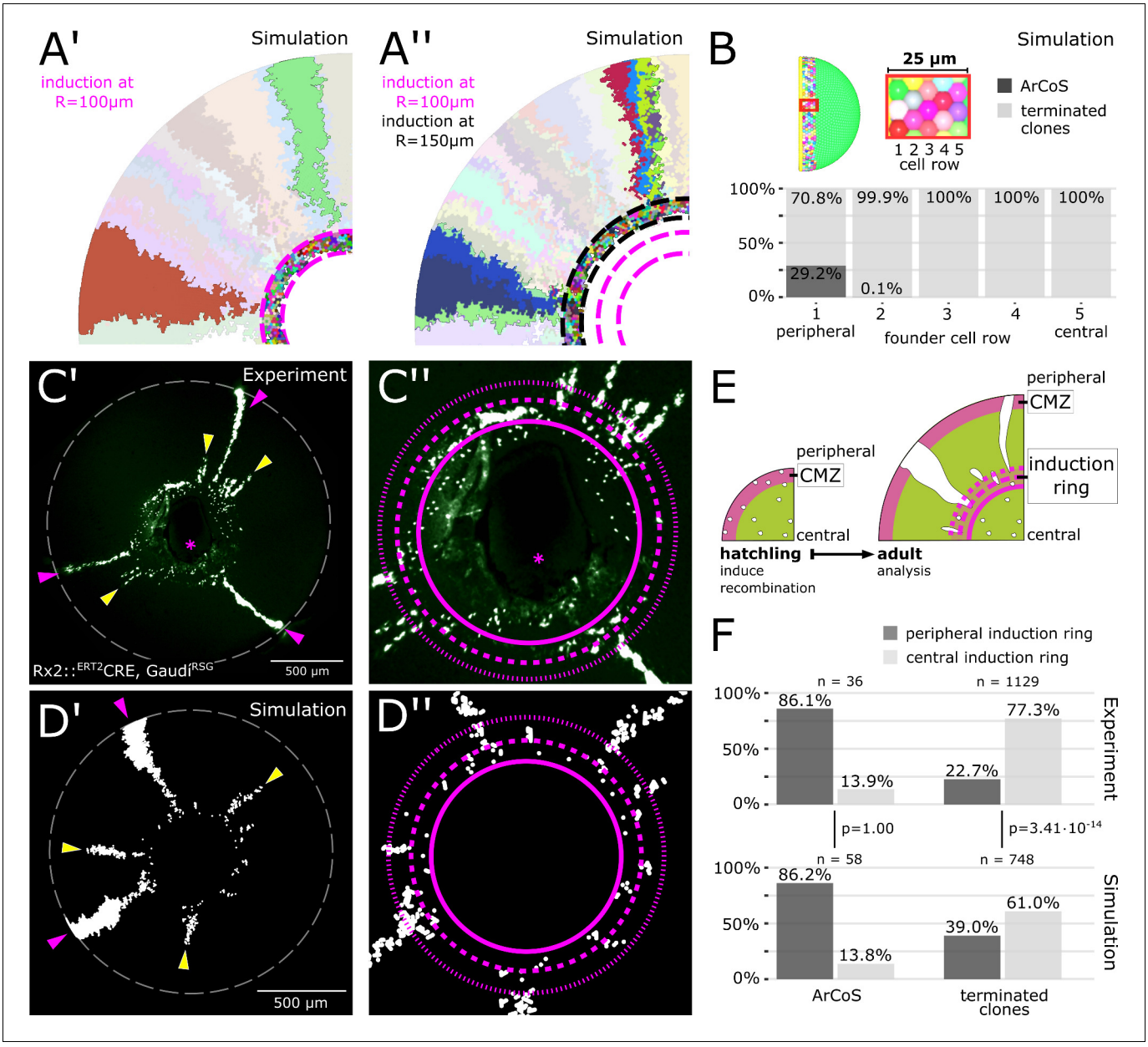

Figure 4. The majority of stem cells differentiates due to cell competition for niche space. (**A'**) Detail of inducer growth mode simulation where clone label was initiated at a radius of R = 100 µm. Small clusters lie centrally, while virtual ArCoS start peripherally. Two virtual ArCoS are highlighted. Pink dashed lines encircle virtual induction ring. (**A''**) Same simulation as in (**A'**), but with clone label initiated at R = 150 µm. The second wave of clonal label leads to a renewed occurrence of small clusters. Two polyclonal patches are highlighted, which correspond to subclones of the highlighted clones in (**A'**). (**B**) The majority of virtual ArCoS derives from stem cells that in simulation step 0 were located in the two most peripheral rows of the virtual CMZ. (**C'**) Proximal view of NR clones. (**C''**) Magnification of central retina from (**C'**). (**C'–C''**) Maximum projection of confocal stack of GFP signal in false colors; rotated to place optic nerve exit (pink asterisk) ventrally. (**D'**) Proximal view of simulated clones. (**D''**) Magnification of central retina from (**D'**). (**C'–D'**) Retinal edge marked by white dashed circle; dashed pink lines encircle and subdivide induction ring into central and peripheral parts; pink arrowheads mark ArCoS, yellow arrowheads mark terminated clones. (**E**) Scheme of the experiment. (**F**) Proportions of ArCoS and terminated clones arising from central and peripheral induction ring in experiment (n = 20 retinae) and simulation (n = 5 simulations, sampled six times each). p-values calculated with a 2-sample test for equality of proportions.

DOI: https://doi.org/10.7554/eLife.42646.026

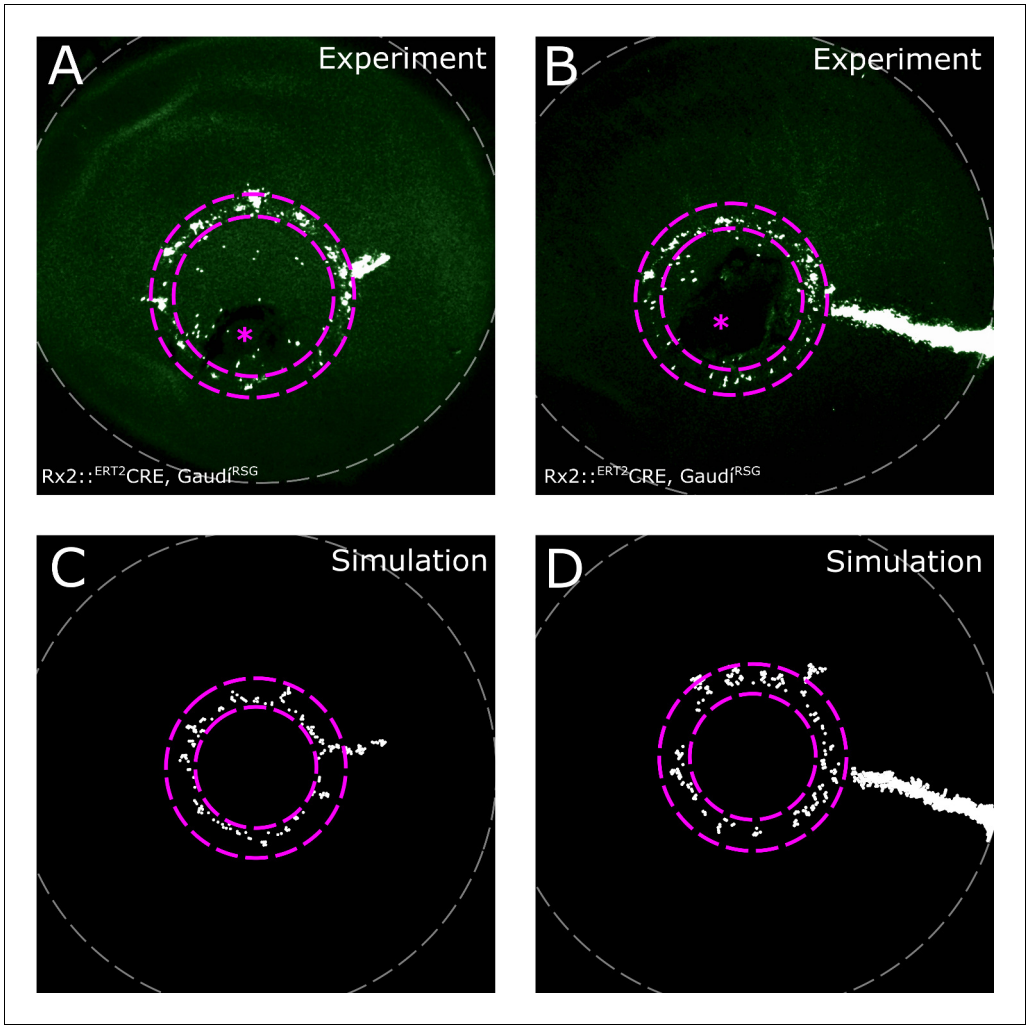

Figure 4—figure supplement 1. Induction ring in very sparsely labelled samples. (**A–B**) Proximal view of NR clones. If label is very sparse, clones occur almost exclusively in the induction ring, with very few or no ArCoS at all, showing that the majority of Rx2-expressing cells form terminated clones. Maximum projection of confocal stack of GFP signal in false colors; rotated to position the optic nerve exit (pink asterisk) ventrally. (**C–D**) Sparse labelling in simulations. Pink dashed lines encircle induction ring, retinal margin marked by white dashed line.

DOI: https://doi.org/10.7554/eLife.42646.027

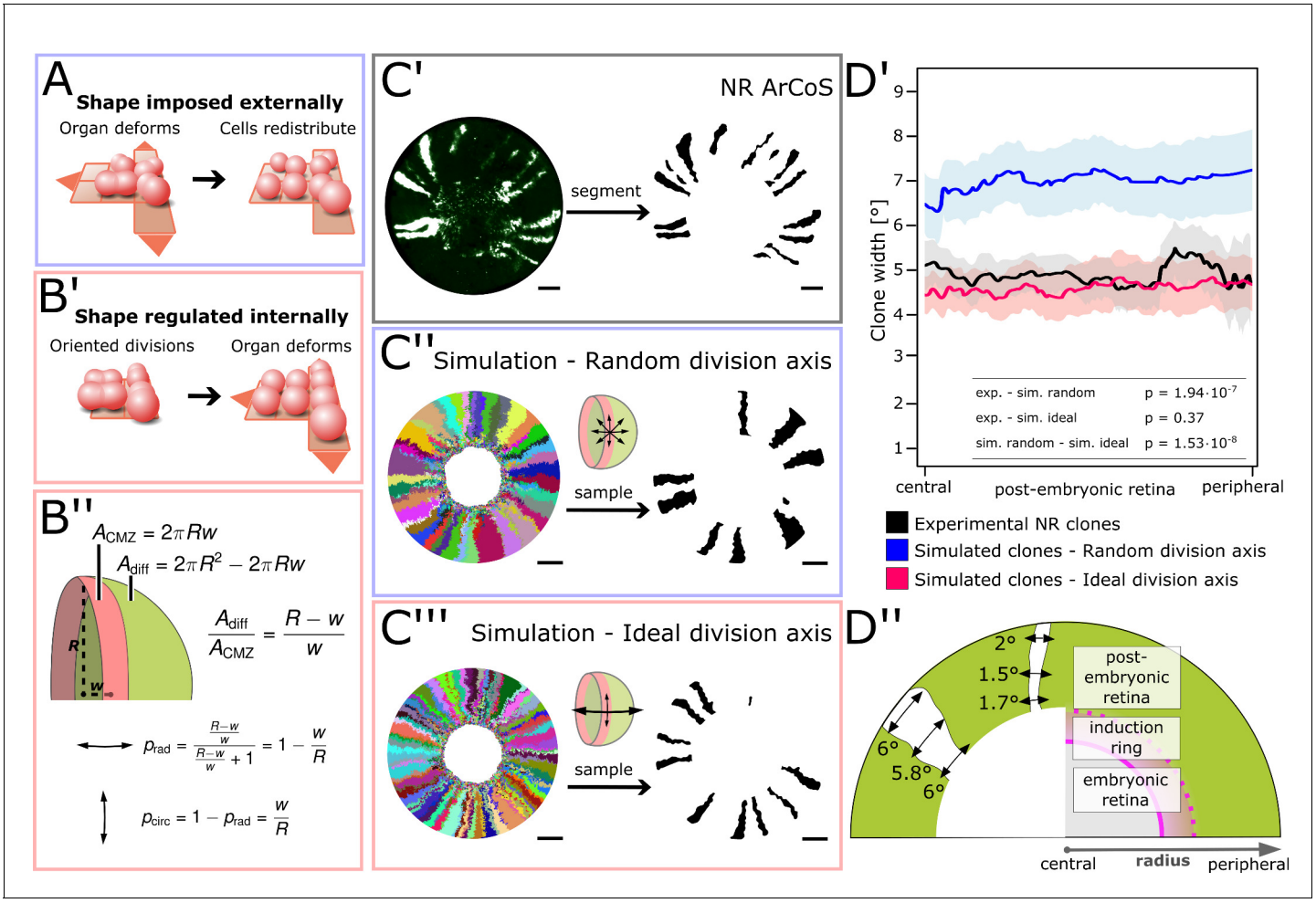

Figure 5. NR stem cells undergo predominant radial divisions as predicted for a shape-giving function. (**A**) If organ shape is imposed externally, then cells in the tissue will distribute to fill the available space. Regardless of cell division axes, organ geometry will lead to a directional growth in stripes. (**B'**) If organ shape is regulated by cell division axes, then oriented divisions are required. (**B''**) If the NR regulates shape through cell divisions, then more divisions along the radial axis are needed to maintain hemispherical geometry. (**C'–C'''**) Examples of experimental and simulated data. For simulations, the full clone population and a random sample are shown. The initial model label was induced at R = 150 µm to match the experimental induction radius. Scale bars: 200 µm. (**D'**) Mean clone width (solid lines) and 95% confidence intervals (shaded) plotted along the post-embryonic retinal radius. Experimental data: n = 99 ArCoS across seven retinae. Simulation, random division axis: n = 102 ArCoS from five simulations; ideal division axis: n = 133 ArCoS from five simulations. p values were calculated with Welch two sample t-test. (**D''**) Schematic of radial compartments of the NR and measurements of clone width in proximal view. The clone width plotted in D' corresponds to the angle enclosed by the clone borders at every radial position.

DOI: https://doi.org/10.7554/eLife.42646.031

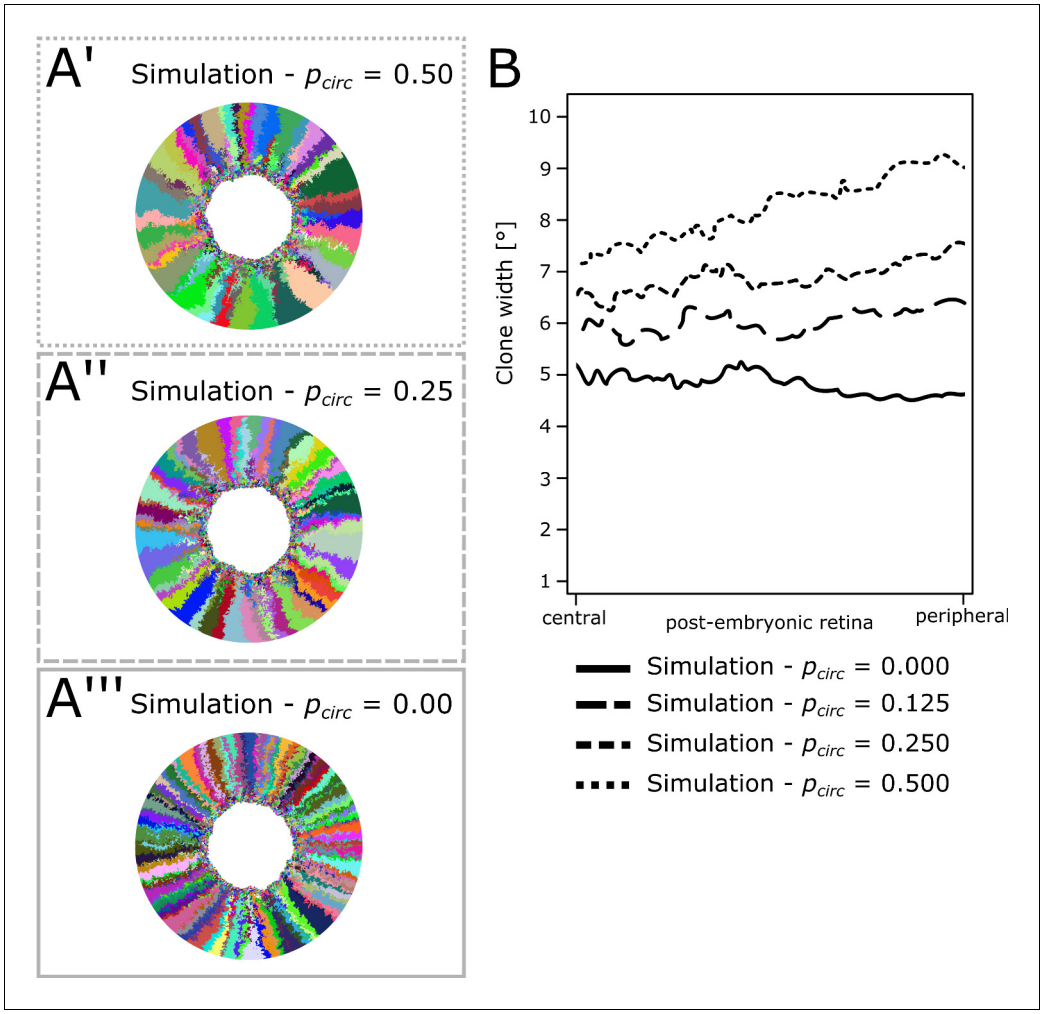

Figure 5—figure supplement 1. Average clone width increases with increasing circumferential divisions. (**A'–A'''**) Example simulations where the probability for circumferential divisions was set to a fixed value of 50% (**A'**), 25% (**A''**), and 0% (**A'''**). (**B**) Average clone width along the post-embryonic radius for circumferential division probability ranging from 0% to 50% (one simulation each).

DOI: https://doi.org/10.7554/eLife.42646.032

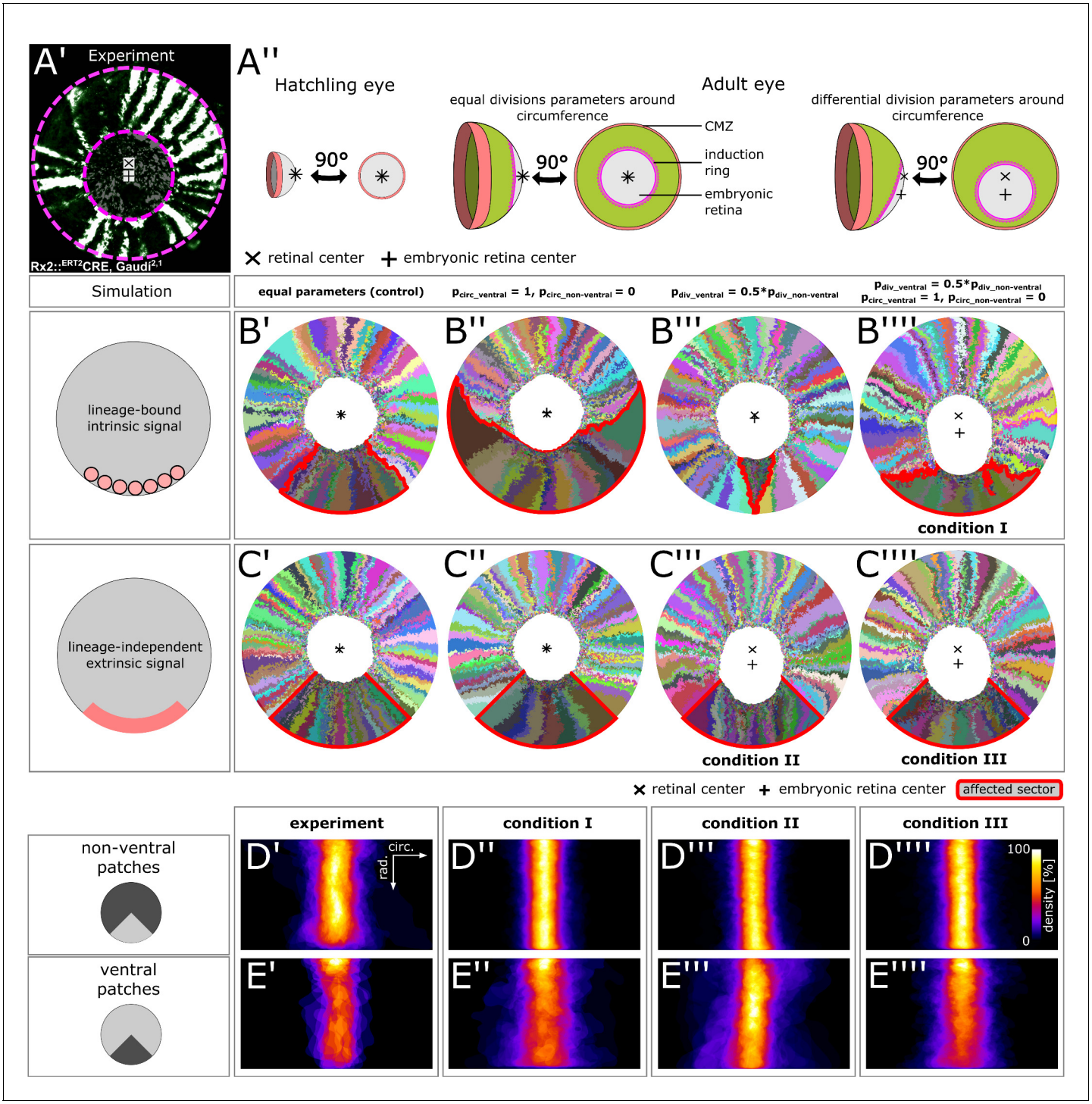

Figure 6. Stem cells in the ventral CMZ have different proliferation parameters. (**A'**) Proximal view of NR clones highlighting the discrepancy between retinal center and embryonic retinal center. Depicted sample is the same as in ***Figure 1D***. (**A''**) A differential proliferative behavior along the CMZ circumference can explain the shift in position of the embryonic retina. (**B'–B''''**) Simulations where lineages whose embryonic origin is in the ventral sector inherit a signal that leads to different proliferation parameters. A shift occurred when ventral lineages had both lower division probability and higher circumferential divisions. Clones originating in ventral embryonic CMZ are outlined in red. (**C'–C''''**) Simulations where all cells in a ventral 90˚ sector exhibit different proliferation parameters regardless of lineage relationships. A shift occurred in conditions with slower proliferation as well as slower proliferation combined with circumferential division axis bias. (**D'–E''''**) Patch superposition for experimental data as well as the three simulated conditions that display a ventral shift of the embryonic retina. (**D'–D''''**) Non-ventral patches. (**E'–E''''**) Ventral patches.

DOI: https://doi.org/10.7554/eLife.42646.035

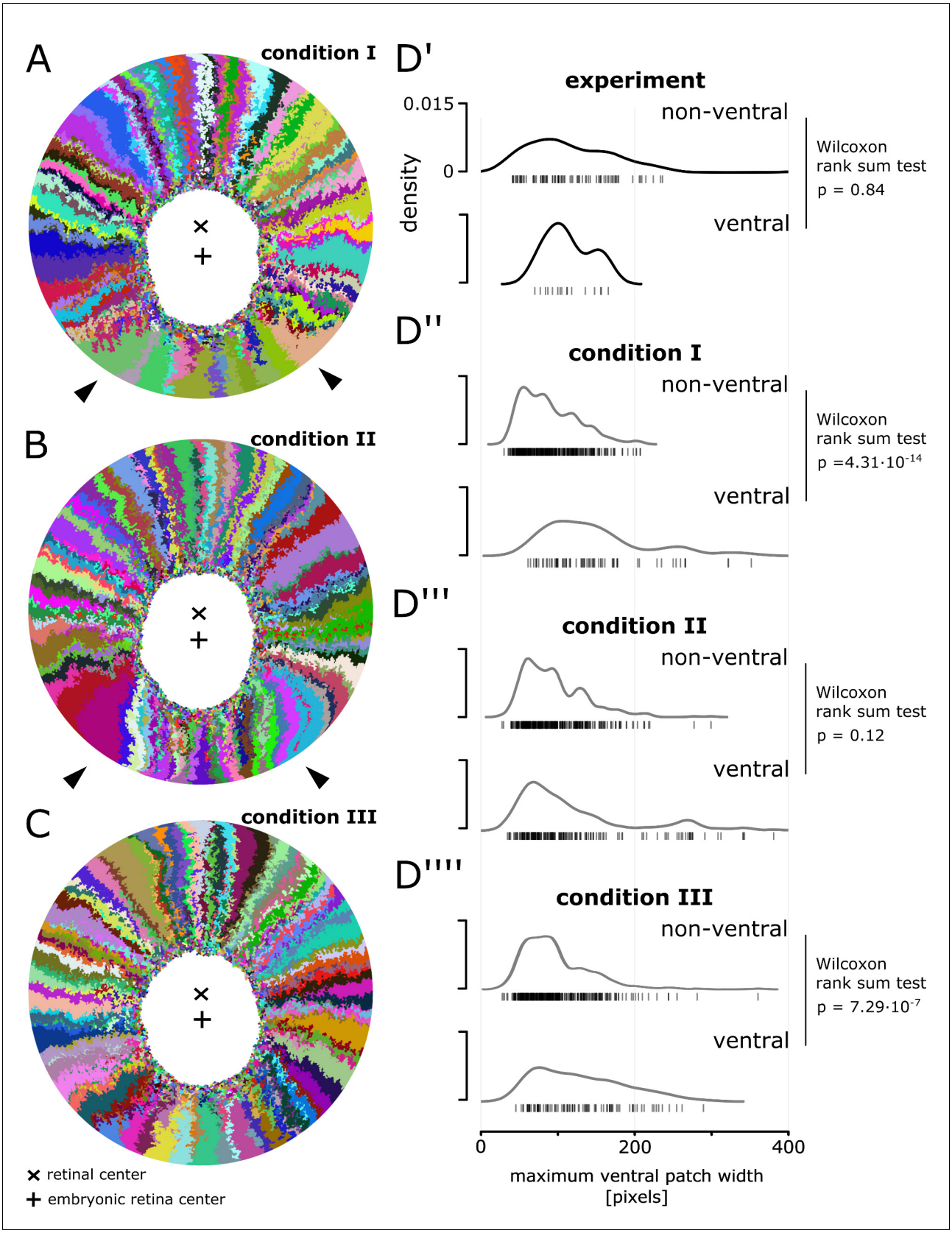

Figure 6—figure supplement 1. Magnification of simulations displaying a ventral shift. (**A**) Magnification of ***Figure 6B''''***. White arrowheads highlight unusually shaped clones with lateral interdigitations. (**B**) Magnification of ***Figure 6C'''***. White arrowheads highlight unusually shaped clones that

Figure 6—figure supplement 1 continued on next page

Figure 6—figure supplement 1 continued

overexpand circumferentially and bend towards the ventral side. (**C**) Magnification of ***Figure 6C''''***. None of the clones display obvious deviations from the average. (**D'–D''''**) Distribution of maximum width of patches that span at least 20% of the radial coordinate.

DOI: https://doi.org/10.7554/eLife.42646.036

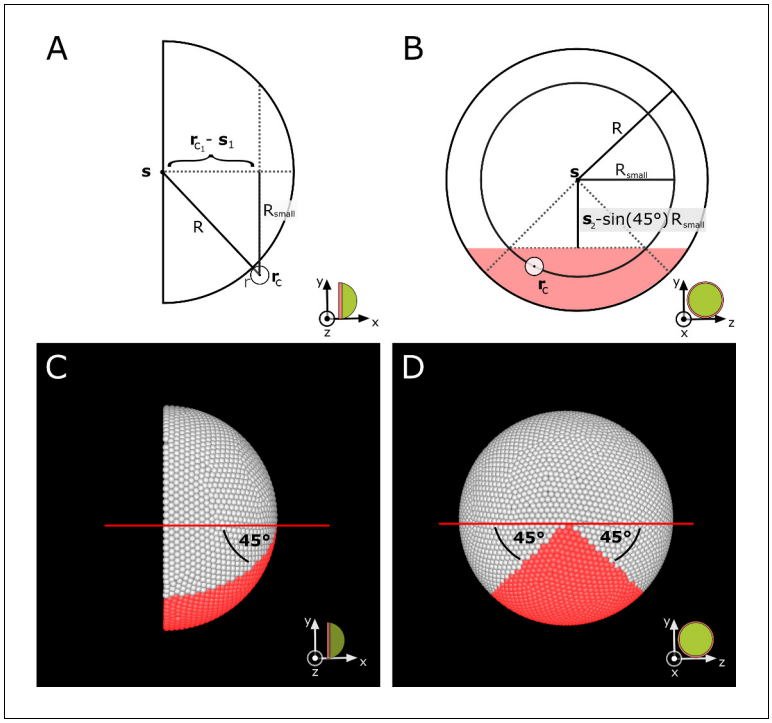

Figure 6—figure supplement 2. Definition of the ventral sector in the simulation. (**A–B**) Schematic side and proximal view showing values used in ***Appendix 1—equations 16-17*** to calculate which cells are located in the ventral sector. For each cell, the corresponding small circle radius R_{small} is calculated. This cell is assigned to the ventral sector if it lies within the red shaded region in (**B**). (**C–D**) Corresponding views in simulation screenshots showing cells in red that satisfy ***Appendix 1—equations 16-17***.

DOI: https://doi.org/10.7554/eLife.42646.037

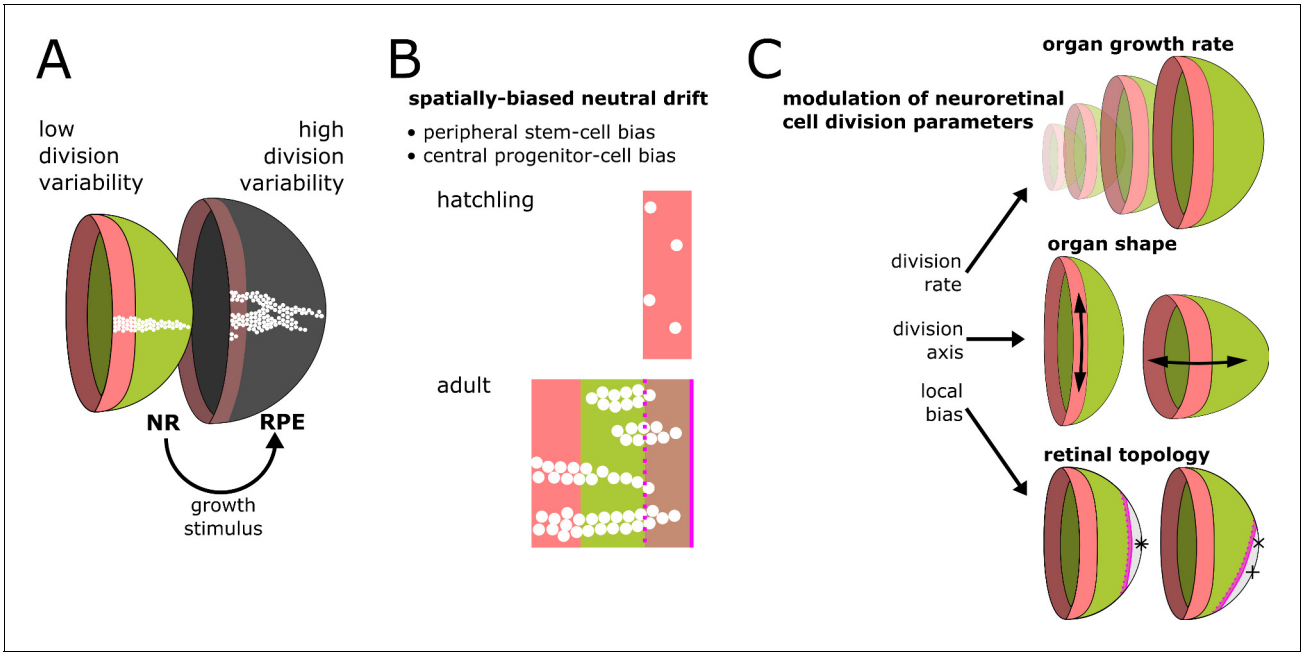

Figure 7. Summary of results and proposed model of CMZ dynamics. (**A**) Growth coordination of NR and RPE is achieved by the NR providing instructive stimuli that modulate proliferation of RPE stem cells. As a result of the different growth strategies, variability in cell division timing is elevated in the RPE and lowered in the NR. (**B**) A base level of variability persists in the NR, such that individual stem cells may differentiate and some multipotent progenitor cells drift to a stem cell fate according to a spatially biased neutral drift model. Thus, stem cells and multipotent progenitor cells have identical proliferative potency. (**C**) Schematic summary of findings and proposed model, where different NR cell proliferation parameters affect both global and local retinal properties.

DOI: https://doi.org/10.7554/eLife.42646.040

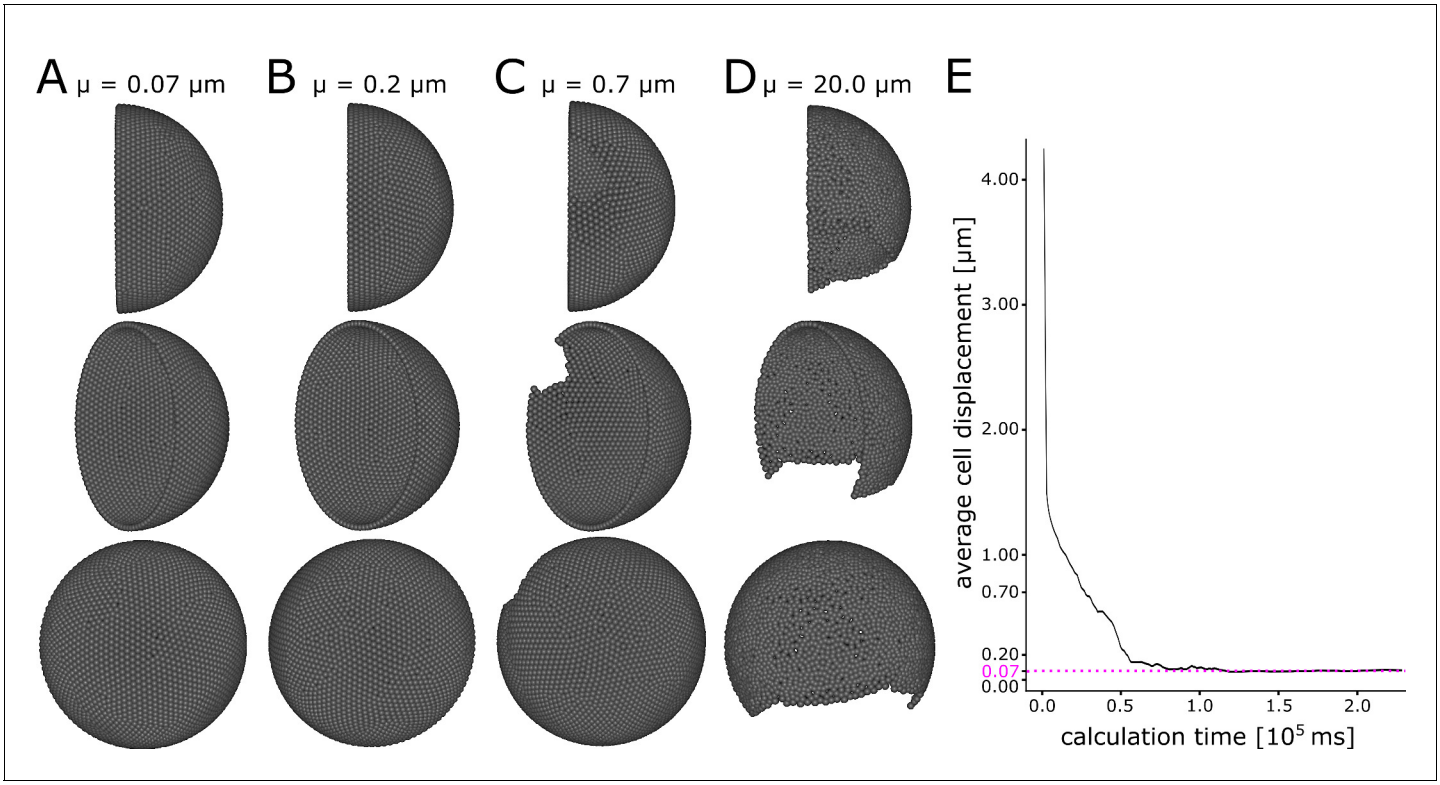

Appendix 1—figure 1. A minimum displacement threshold μ = 0.2 ensures even cell distribution. Different views of initial condition of the simulation with (**A**) μ = 0.07 μm, (**B**) μ = 0.2 μm, (**C**) μ = 0.7 μm, (**D**) μ = 20.0 μm. (**E**) Calculation time plotted against the average cell displacement during initialization of the simulation. The simulation converges to 0.07 μm average displacement (pink dashed line).

DOI: https://doi.org/10.7554/eLife.42646.048

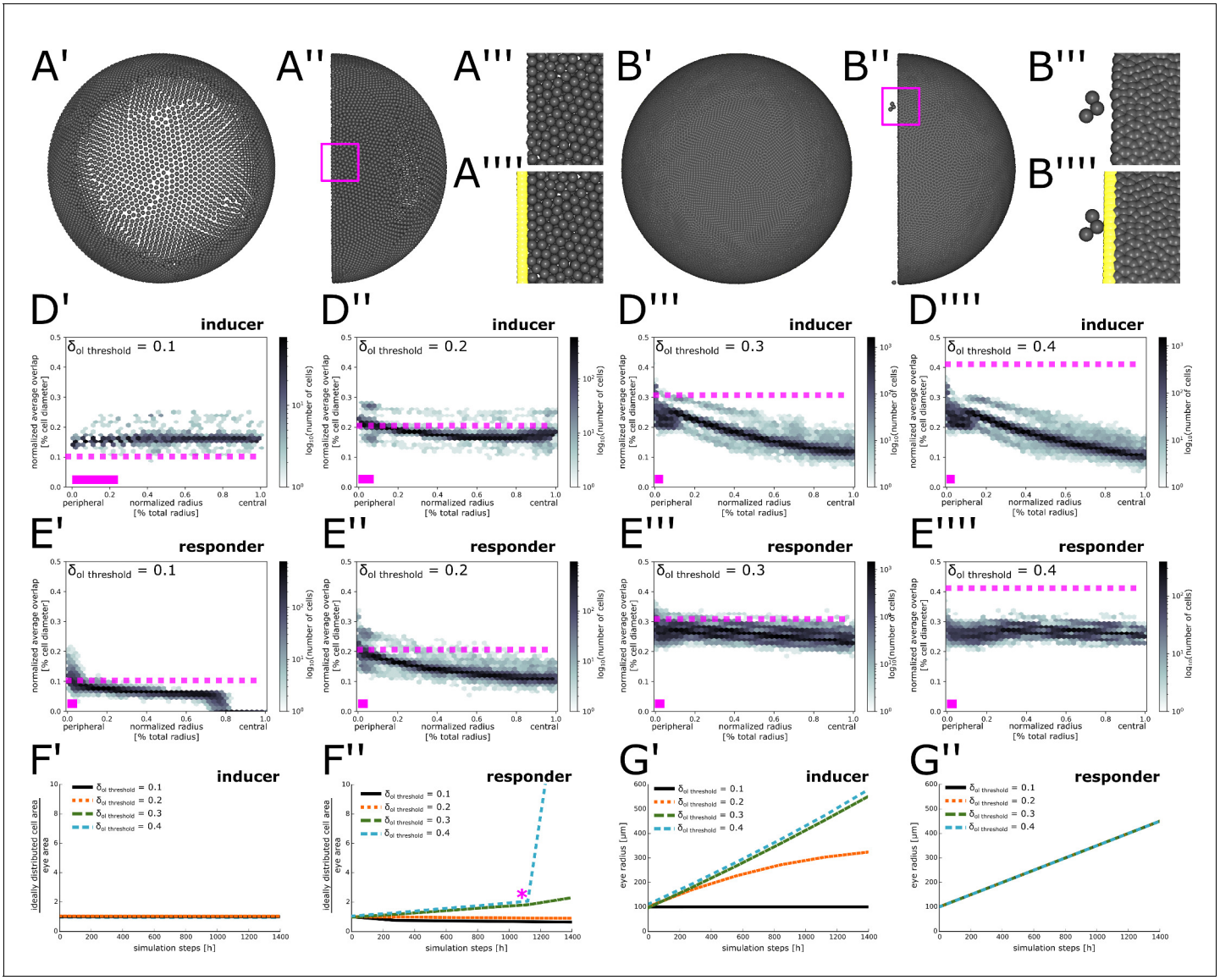

Appendix 1—figure 2. Parameter scan to determine optimal overlap threshold values. (**A'–B''''**) Different views of representative simulations lacking coupling between eye radius growth and cell proliferation. (**A'–A''**) Eye area growth rate exceeds cell proliferation rate, resulting in cell dispersion. (**A'''–A''''**) Magnification of inset in (**A''**) showing peripheral cells without (**A'''**) or with (**A''''**) obstacle cells displayed. (**B'–B''**) Cell proliferation rate exceeds eye area growth rate, resulting in extremely dense cell packing. (**B'''–B''''**) Magnification of inset in (**B''**) showing peripheral cells without (**B'''**) or with (**B''''**) obstacle cells displayed. Three cells have squeezed through the obstacle cell layer. (**D'–E''''**) Normalized average overlap of cells at simulation step 1400 plotted against their position along the normalized radius. Dashed pink line: Value of $\delta_{\mathrm{ol\_threshold}}$ used for the respective simulation. Solid pink bar: Extent of virtual CMZ. (**D–D''''**) inducer growth mode; (**E'–E''''**) responder growth mode. (**F'–F''**) Ratio between total area required by cells and total eye area from simulation step 0 to simulation step 1400 for different values of $\delta_{\mathrm{ol\_threshold}}$. (**F'**) inducer growth mode; (**F''**) responder growth mode. Pink asterisk marks approximate time when cells start squeezing through obstacle cell layer. (**G'–G''**) Growth of the eye radius from simulation step 0 to simulation step 1400 for different values of $\delta_{\mathrm{ol\_threshold}}$. (**G'**) inducer growth mode; (**G''**) responder growth mode.

DOI: https://doi.org/10.7554/eLife.42646.049

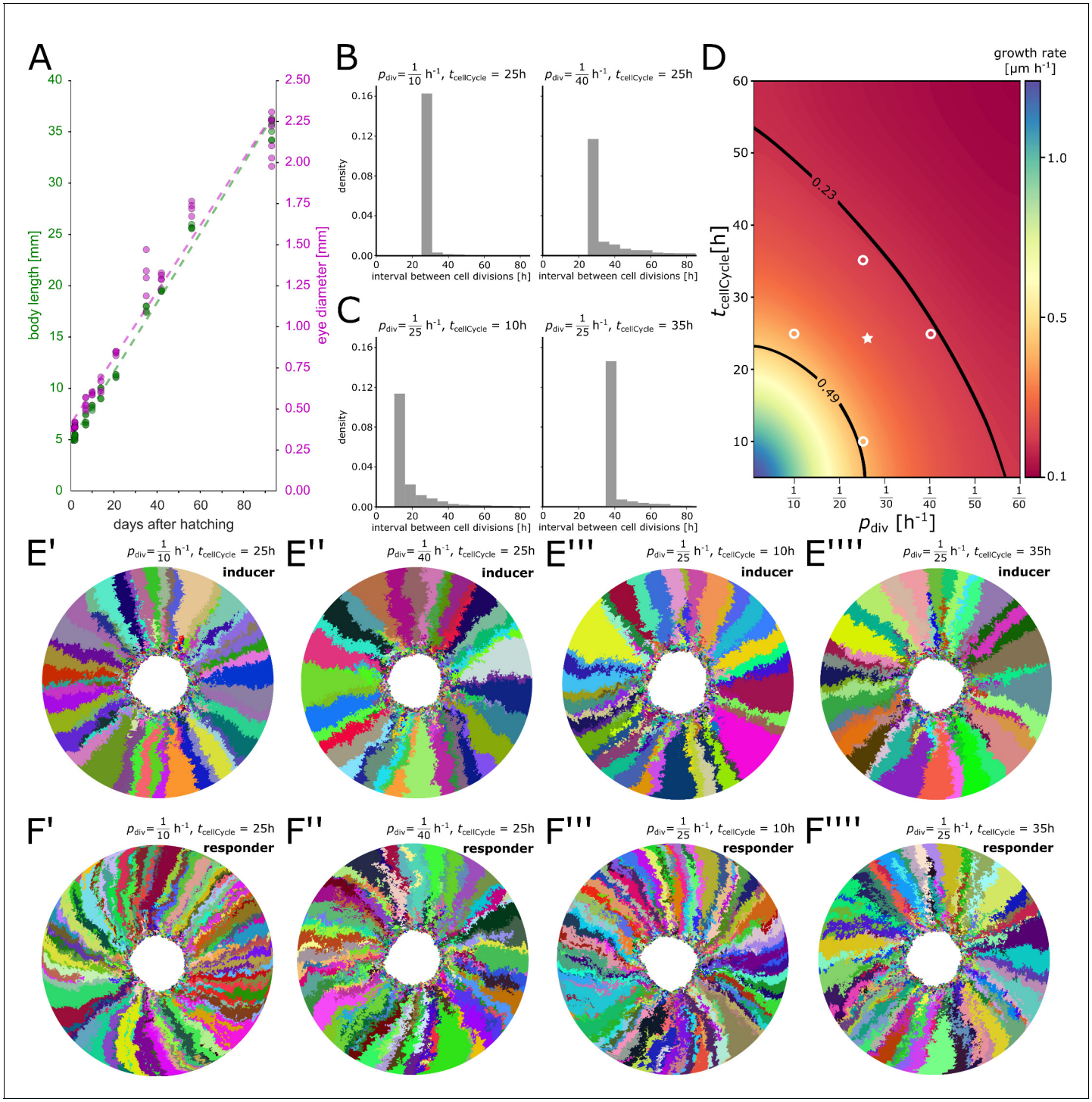

Appendix 1—figure 3. Parameter scan of minimum cell cycle and division probability. (**A**) Experimental data. Both body length (green) and eye diameter (magenta) grow approximately linearly over the first 90 days after hatching. (**B**) Distribution of cell division intervals with fixed $t_{\text{cellCycle}}$ and variable p_{division}. (**C**) Distribution of cell division intervals with variable $t_{\text{cellCycle}}$ and fixed p_{division}. (**D**) Eye growth rates in the simulation determined from a parameter scan of $t_{\text{cellCycle}}$ and p_{division} entailing over 150 simulation runs; intermediate values were interpolated. The plausible parameter space estimated from experimental measurements is contoured by black lines. Open white circles represent values for simulations depicted in (**B, C, E'–E'''', F'–F''''**). White star represents values used for simulations in the main manuscript. (**E'–E''''**) Representative simulations of the inducer growth mode at different values for $t_{\text{cellCycle}}$ and p_{division}. (**F'–F''''**) Representative simulations of the responder growth mode at different values for $t_{\text{cellCycle}}$ and p_{division}. Throughout the figure p_{division} is abbreviated as p_{div}.

DOI: https://doi.org/10.7554/eLife.42646.050